

Dramatic Enhancement of Supercontinuum Generation in H₂O by Non-Harmonic Two-Color Excitation

TSUNETO KANAI^{1,*}, CHENGXIANG JIN^{1,2}, HIBIKI TSUNEKAWA^{1,2}, ATSUNORI SAKURAI^{1,2,3}, AND TOSHIKI SUGIMOTO^{1,2,3}

¹Institute for Molecular Science, National Institutes of Natural Sciences, Okazaki, Aichi 444-8585, Japan

²Graduate Institute for Advanced Studies, SOKENDAI, Okazaki, Aichi 444-8585, Japan

³Laser-Driven Electron-Acceleration Technology Group, RIKEN SPring-8 Center, Sayocho, Hyogo 679-5148, Japan

*goldwell74@gmail.com

Compiled August 19, 2025

We demonstrate a dramatic enhancement of supercontinuum generation (SCG) in H₂O driven by non-harmonic two-color laser fields, where pump and seed frequencies are not integer multiples. This scheme yields a broadband SC spectrum enhanced by approximately three orders of magnitude over the single-color case. Systematic experiments and theoretical analysis, including isotope effects, show that the enhancement arises from soliton compression with resonant dispersive wave (RDW) emission, phase- and group-velocity-matched four-wave mixing (FWM), and cross-phase modulation (XPM), offering a versatile route to stronger SCG and noise suppression in broadband spectroscopy in H₂O, an emerging topic in attosecond and surface physics.

<http://dx.doi.org/10.1364/ao.XX.XXXXXX>

SCG from intense ultrashort pulses in transparent media is a key light source in ultrafast optical science [1–6], supporting applications including seed sources for optical parametric amplifiers (OPAs) [7, 8], time-resolved spectroscopy [9], frequency combs [10], nonlinear microscopy [11], and lightwave engineering [12]. Recent high-power mid-infrared (mid-IR) laser systems, especially those using SCG from picosecond pulses as a seed [7, 8], have expanded the scope of SCG beyond conventional $\chi^{(3)}$ -based processes into high-order and strongly nonperturbative phenomena such as high harmonic generation (HHG) [13–15] and high-order frequency conversion [16]. The interplay between HHG and SCG has attracted growing interest.

Harmonics-enhanced SCG [17–22], a representative example of this interplay, has been extensively explored using two-color filamentation schemes with a second harmonic (SH) [20, 23–26]. When the SH field efficiently breaks inversion symmetry [27], this configuration can enable efficient SCG from the THz to soft-x-ray region [23–26]. In contrast, few studies have explored two-color fields with non-integer frequency ratios, termed *non-harmonic two-color fields* here [8, 15, 28–32]. Prior work demonstrated tunable visible pulses via FWM in gases [28] and broadband sidebands via cascaded FWM in BBO [30], but systematic studies in liquids are scarce: Most recently, Junaid *et al.* investi-

gated single and cascaded FWM as well as stimulated Raman scattering (SRS) in liquid-core fibers using continuous-wave and picosecond laser sources [29].

In this Letter, we demonstrate a dramatic enhancement (DE) of SCG in H₂O using non-harmonic two-color laser fields. Compared to single-color or harmonic excitation, this configuration can yield much stronger SCG. Systematic experiments and theoretical analysis, including isotope effects, reveal that the enhancement originates from a synergistic interplay among soliton compression accompanied by RDW emission [33–38], phase- and group-velocity-matched FWM [39], and subsequent cascaded FWM and XPM. These findings not only introduce a versatile approach to achieving broader and more intense SCG, but also provide an effective means of suppressing the background noise signal, an inherent issue in broadband/multicolor spectroscopy in liquids—particularly in H₂O, an emerging topic in attosecond science [38, 40] and surface/interface physics [41, 42].

The experiments employed a Yb:KGW chirped-pulse amplification laser system (CARBIDE-CB3, Light Conversion Ltd.) delivering 180-fs, 1036-nm pulses at up to 400 μ J and 2 MHz, while we operated the system at 40 μ J and 100 kHz for this study. The output beam was split into two parts: one part, equipped with a delay line, served as the pump for the two-color SCG experiments, while the other, driving an OPA (ORPHEUS-F, *ibid*), was used to generate the seed for these experiments, producing 640–940 nm and 1.15–2.5 μ m pulses with durations of 40–80 fs and energies of 0.4–1.6 μ J. The pump and seed beams were spatially overlapped using dichroic mirrors and focused collinearly into the center of a 7.4-mm-thick layer of liquid H₂O or its isotopologue D₂O, sandwiched between 1.3-mm-thick fused silica windows, by a lens with a focal length of 150 mm. Neutral density filters were used to control the pulse energy of each beam, and telescopic lens systems were inserted into both beam paths to ensure nearly identical focal spot sizes, with a $1/e^2$ radius w_0 of approximately 34 μ m in H₂O and D₂O. The peak power of the pump was typically set to 4.2 MW by adjusting the pulse energy to 800 nJ, $\approx 67\%$ of the critical power for filamentation, $P_{\text{cr}} = 3.77\lambda^2/(8\pi n_0 n_2)$ (theoretically predicted by Marburger [6] and experimentally demonstrated by Liu and Chin [5]), which amounts to 6.3 MW for H₂O assuming $n_2 = 1.9 \times 10^{-16}$ cm²/W [43]. The generated SC spectra were

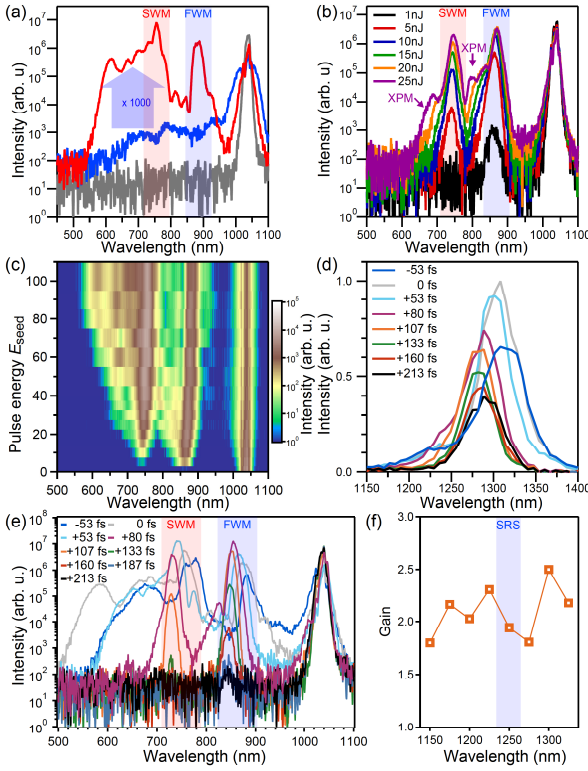


Fig. 1. (a) SC spectra generated in H₂O (red), showing strong enhancement when driven by both the pump (1036 nm, 800 nJ) and seed (1300 nm, 100 nJ) pulses. For comparison, single-color SC spectra are shown for the same pump energy (800 nJ, gray) and for an increased pump energy (1200 nJ, blue). (b, c) Dependence of the SC spectra on the seed pulse energy E_{seed} in the low-energy regime [1–25 nJ, (b)] and over an extended range up to 100 nJ (c). (d, e) SC spectra measured using a Si-based spectrometer (d), and amplified seed spectra measured using an InGaAs-based spectrometer (e), in H₂O at various time delays τ (from -53 fs to +213 fs). Distinct spectral peaks attributed to SWM and FWM are observed in the SWM and FWM regions, respectively. (f) Spectral gain of the seed pulse, defined as the output-to-input intensity ratio, plotted as a function of λ_{seed} in H₂O.

recorded by collecting Fresnel reflections from a fused silica prism with InGaAs-based (NIRQuest-256, Ocean Optics Inc.; 900–2500 nm) and Si-based (LR1, Aseq Instruments; 200–1100 nm) spectrometers.

We consider generalized FWM between an intense pump and a weak seed, along with its cascaded processes. When the seed frequency is an integer multiple of the pump ($\omega_{\text{seed}} = q\omega_{\text{pump}}$, $q \in \mathbb{Z}$, $q \geq 2$), as in harmonics-enhanced SCG, the FWM-generated waves ($\omega_{\text{FWM}} = |q \pm 2|\omega_{\text{pump}}$, $|2q \pm 1|\omega_{\text{pump}}$) retain harmonic relationships with the pump. Here, four-wave rectification [23, 24, 26] is regarded as the case “ $\omega_{\text{FWM}} = 0$ ” with $q = 2$. Consequently, higher-order processes dominantly realized through its cascading, such as effective six-wave mixing (SWM) and eight-wave mixing (EWM), also generate only harmonically related frequencies. In contrast, for non-harmonic pump-seed pairs, the generated frequencies become intrinsically non-harmonic, dramatically increasing the number of accessible frequency components. This enhanced effect is analogous to the generation of dissonance by two non-harmonic sounds. When one sets $\omega_{\text{pump}}/2 < \omega_{\text{seed}} < \omega_{\text{pump}}$, degenerate FWM generates an idler—not to be confused with the idler of OPAs—on

the anti-Stokes side at $\omega_{\text{FWM}}^{\text{as}} = 2\omega_{\text{pump}} - \omega_{\text{seed}}$, which seeds further non-degenerate FWM-based cascaded processes with non-harmonic frequencies: $\omega_{\text{SWM}}^{\text{as}} = \omega_{\text{FWM}}^{\text{as}} + \omega_{\text{pump}} - \omega_{\text{seed}} = 3\omega_{\text{pump}} - 2\omega_{\text{seed}}$ and $\omega_{\text{EWM}}^{\text{as}} = \omega_{\text{SWM}}^{\text{as}} + \omega_{\text{pump}} - \omega_{\text{seed}} = 4\omega_{\text{pump}} - 3\omega_{\text{seed}}$. Here, the idlers on the anti-Stokes side are much stronger than those on the Stokes side, while the relative magnitude relationship is reversed in the conjugated case, $2\omega_{\text{pump}} > \omega_{\text{seed}} > \omega_{\text{pump}}$.

The perturbative understanding described above, however, captures only part of the observed phenomena. In fact, a DE in SCG in H₂O was successfully demonstrated using a non-harmonic two-color field, comprising a pump (1036 nm, 800 nJ) and a seed (1300 nm, 100 nJ) [Fig. 1(a)]. The above perturbative picture predicts cascaded FWM processes with discrete spectral components at $\lambda_{\text{FWM}}^{\text{as}} = 861$ nm, $\lambda_{\text{SWM}}^{\text{as}} = 737$ nm, and $\lambda_{\text{EWM}}^{\text{as}} = 644$ nm. Hereafter, we refer to the spectral range $\lambda_i^{\text{as}} \pm 40$ nm as the “*i* region”. Under the optimized condition used in Fig. 1(a), however, a broadband enhancement about three orders of magnitude was observed in the 600–800 nm range, compared to the optimized single-color case, despite the latter employing a pump pulse with 1.5 times higher energy (1200 nJ, $1P_{\text{cr}}$). Notably, although the seed pulse energy was only 100 nJ, the seed played a dramatic role in enabling broadband SCG, as evidenced by comparison with the spectrum obtained using the pump pulse alone at the same energy (800 nJ) [Fig. 1(a)].

The key features of the underlying physics can be elucidated by examining the dependence of the SC spectrum on the seed pulse energy E_{seed} , while keeping the pump energy fixed at 800 nJ. As shown in Fig. 1(b), even very weak seed pulses initiated nonlinear effects: FWM appeared at $E_{\text{seed}} = 1$ nJ, and SWM at 5 nJ, accompanied by an increase of more than two orders of magnitude in the FWM intensity. This nonlinear increase cannot be explained by perturbative FWM, which is a linear process with respect to the seed, as discussed later. The FWM signal began to saturate around 15 nJ, indicating that significant part of the pump energy was transferred to the SWM process via the cascaded FWM rather than direct SWM. Also around this seed energy (15 nJ), spectral broadening of the FWM and the SWM signal occurred. Interestingly, this broadening showed a clear asymmetry toward shorter wavelengths, suggesting dominance of XPM induced by the falling edge of the pump pulse with larger group velocity than FWM and SWM [Fig. 2(b)], rather than self-phase modulation (SPM), which typically results in symmetric broadening. Figure 1(c) shows the SC spectrum as a function of E_{seed} up to 100 nJ, the stability limit for SCG. The broadest spectrum was obtained at around 100 nJ, as also shown in Fig. 1(a), whereas intuitively expected broadening into broadband light via EWM and XPM was not observed.

The delay (τ) dependence of SCG in H₂O is shown in Figs. 1(d,e), where τ is defined as the pump-seed delay, with $\tau > 0$ indicating that the pump precedes the seed. The zero delay ($\tau = 0$) is defined as the condition where the SC spectral cutoff reaches its maximum extent, and the same pulse parameters as in Fig. 1(a) were used. As expected, clear seed amplification associated with FWM was observed for $|\tau| \lesssim 160$ fs [Fig. 1(d)], accompanied by the synchronized emergence of FWM and SWM components [Fig. 1(e)]. The FWM and SWM signals exhibit a red shift that increases with τ , an effect attributed to the positive chirp of the pump induced by SPM [Fig. 1(e)]. In contrast, the center frequency of the seed was blue-shifted for $\tau > 0$ relative to that at $\tau = 253$ fs (virtually no temporal overlap), whose red spectral component was already absorbed by the second

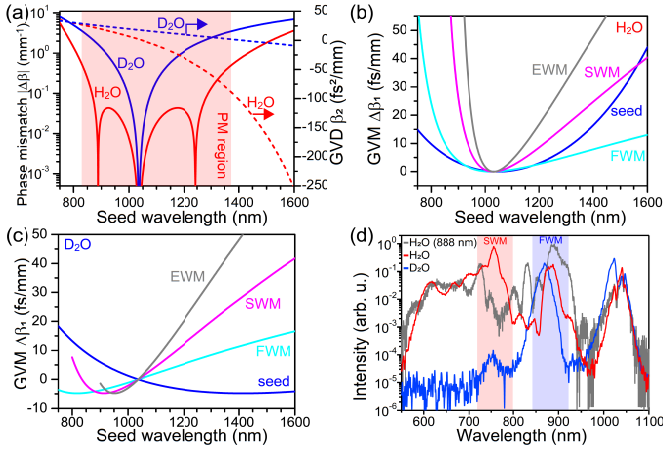


Fig. 2. (a) The absolute value of the phase mismatch $|\Delta\beta|$ for degenerate FWM ($\omega_{\text{FWM}} = 2\omega_{\text{pump}} - \omega_{\text{seed}}$) in H₂O (solid red) and D₂O (solid blue), along with the GVD β_2 of H₂O (dotted red) and D₂O (dotted blue) [45], plotted as functions of λ_{seed} . The PM condition in H₂O is satisfied at $\lambda_{\text{seed}} = 1243$ nm and 888 nm. The ZDW of H₂O and D₂O are 1048 nm [39] and 1415 nm, respectively. The wavelengths of maximum group velocity are slightly offset from the ZDWs, appearing at 1051 nm for H₂O and 1411 nm for D₂O, due to the finite second derivative $d^2n/d\lambda^2$. (b, c) GVM between the pump and the FWM (cyan), SWM (magenta), EWM (gray), and seed (blue) pulses, plotted as functions of λ_{seed} in H₂O (b) and D₂O (c). Group velocity matching between the FWM and seed pulses is satisfied at $\lambda_{\text{seed}} = 1176$ nm and 926 nm for H₂O. (d) SC spectra generated in H₂O (red) and D₂O (blue) using $\omega_{\text{pump}} = 1036$ nm, 800 nJ and $\omega_{\text{seed}} = 1300$ nm, 100 nJ. For comparison, the SC spectrum generated using the same pump and a conjugate seed (888 nm, 100 nJ), which satisfies the PM condition, is also shown (gray).

overtone or combination band of the OH stretching vibration in H₂O centered at 1450 nm. For $\tau < 0$, the seed was red-shifted owing to its negative chirp induced by H₂O, combined with amplification via FWM and soliton compression, as evidenced by the spectral broadening observed at $|\tau| \lesssim 53$ fs [Fig. 1(d)]. The seed gain of 2.5 was measured at $\lambda_{\text{seed}} = 1300$ nm, with no significant dependence on wavelength [Fig. 1(f)]. This suggests that the amplification primarily results from degenerate FWM, rather than from SRS involving, for example, the bending mode of H₂O at 1650 cm⁻¹, which can be resonantly excited at $\lambda_{\text{seed}} \approx 1250$ nm [44].

The observed dominance of FWM over SRS in H₂O in Fig. 1(f) can be understood in terms of phase-matching (PM) of FWM [29, 46]. Figure 2(a) presents the absolute value of the phase mismatch $|\Delta\beta|$ for degenerate FWM, alongside the group velocity dispersion (GVD) β_2 of H₂O and D₂O, plotted as functions of the seed wavelength. Notably, the PM condition in H₂O is satisfied at $\lambda_{\text{seed}} = 888$ and 1243 nm, the latter close to the SRS resonance near $\lambda_{\text{seed}} = 1250$ nm, effectively dominates SRS gain. Here, we refer to the region with $|\Delta\beta| \lesssim 0.5$ mm⁻¹ for H₂O as the PM region (830 nm $< \lambda_{\text{seed}} < 1375$ nm).

The effect of PM of FWM is, in the present case, significantly enhanced by the group velocity matching. Figures 2(b,c) show the group velocity mismatch (GVM) between pulse i ($i = \text{FWM, SWM, etc.}$) and the pump, $\Delta\beta_1^{i,\text{pump}} := 1/v_g^i - 1/v_g^{\text{pump}}$,

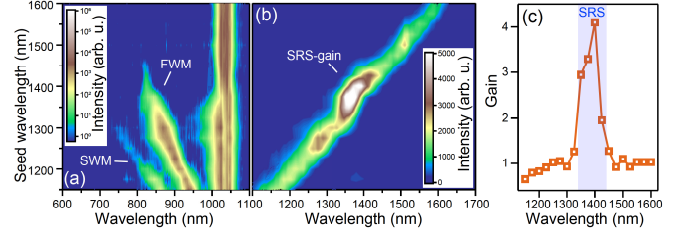


Fig. 3. (a, b) SC spectra generated in D₂O as functions of λ_{seed} , measured using (a) a Si-based and (b) an InGaAs-based spectrometer. (c) Total gain of the seed pulse in D₂O, plotted as a function of λ_{seed} . In all measurements, the pump and seed pulse energies are fixed at $E_{\text{pump}} = 800$ nJ and $E_{\text{seed}} = 100$ nJ, respectively.

in H₂O (b) and D₂O (c) as functions of λ_{seed} . Here, v_g^j denotes the group velocity of pulse j . In H₂O, group velocity matching between the seed and FWM signals is satisfied at $\lambda_{\text{seed}} = 1176$ nm and 926 nm. $\Delta\beta_1^{\text{seed,pump}}$ and $\Delta\beta_1^{\text{FWM,pump}}$ in the PM region remains sufficiently small (< 15 fs/mm), relative to the pump pulse duration of 180 fs and the observed maximum filamentation length (≈ 2 mm), thereby enhancing the parametric FWM process in H₂O. For D₂O, on the other hand, phase mismatch is significantly larger than that in H₂O [Fig. 2(a)], and no spectral enhancement was observed, as shown in Fig. 2(d). This observation is counterintuitive, when focusing only on its higher nonlinear refractive index n_2 (6.4×10^{-16} cm²/W [43]) compared to that of H₂O (1.9×10^{-16} cm²/W [43] or 4.1×10^{-16} cm²/W [47]).

In addition to PM and GVM, soliton dynamics plays crucial role in this DE process. The zero-dispersion wavelengths (ZDWs) of H₂O (1048 nm) indicates that the seed wavelength at 1300 nm lies in the anomalous dispersion regime of H₂O, suggesting the possibility of soliton compression during the amplification via FWM accompanied by RDW emission [33–38]. To logically isolate this effect, we reversed the roles of the seed and idler waves in FWM in Fig. 2(d) by employing a seed at 888 nm, which also satisfies the PM condition to efficiently generate a FWM idler around 1243 nm. The gray curve in Fig. 2(d) shows the SC spectrum obtained with this conjugate wavelength condition. Despite the stronger amplified seed in the FWM region observed in this case, which is advantageous for generating the SWM component through cascaded FWM, a marked suppression in the SWM region is evident [Fig. 2(d)]. In contrast, a DE is observed in the 600–730 nm range, similar to the results before applying conjugation. This indicates that the spectral component in this range does not originate from the cascaded FWM process, but rather suggests the presence of another mechanism.

The two fundamental parameters of RDW emission strongly support that RDW emission is the responsible mechanism. In fact, the PM condition for RDW emission, $\beta(\omega_{\text{RDW}}) = \beta(\omega_{\text{seed}}) + (\omega_{\text{RDW}} - \omega_{\text{seed}})/v_g^{\text{seed}}$, yields $\lambda_{\text{RDW}} = 666$ nm, which corresponds to the center of the observed 600–730 nm range. The soliton order, on the other hand, $N = \sqrt{\gamma P_0 T_0^2 / |\beta_2|}$, was estimated to be $N \approx 1.2$, using $T_0 = 36$ fs (characteristic pulse duration at 1300 nm), $P_0 \approx 2.4$ MW (peak power of a 2.5-times-amplified 100 nJ seed after 39% absorption in H₂O), and $\gamma = 2\pi n_2 / (\lambda_0 A_{\text{eff}})$ with $A_{\text{eff}} = \pi w_0^2$. This value satisfies the condition for RDW emission, and indeed, significant spectral broadening of the seed is observed for $|\tau| \lesssim 53$ fs in Fig. 1(d) accompanied by the enhanced signal observed 600–730 nm range

in Fig. 1(e). Here, the FWM process $2\omega_{\text{FWM}} - \omega_{\text{seed}}$, which could also generate spectral component in this region, is expected to make only a minor contribution due to the large phase mismatch ($\approx 36 \text{ mm}^{-1}$), which is likely the origin of the spectral modulation observed in this range. For pulse-duration measurements of SC, however, phase stabilization of each pulse is required, and modifications to the experimental setup are currently in progress.

Finally, we return to the issue of competition between FWM and SRS. Figure 3(a,b) shows the SCG spectra generated in D_2O as functions of λ_{seed} . The pulse energies of the seed and pump are identical to those used in Fig. 1(a). A clear enhancement is observed at $\lambda_{\text{seed}} = 1350\text{--}1425 \text{ nm}$, which corresponds to resonance with the stretching mode of D_2O ($2300\text{--}2700 \text{ cm}^{-1}$). The gain reaches 4.1 at 1400 nm [Fig. 3(c)]; however, no enhancement is observed for FWM or SWM. In contrast to the H_2O case [Fig. 1(f)], SRS dominates over FWM in D_2O because of the large phase-mismatch for FWM and the high gain coefficient of SRS [29, 46].

In summary, we have demonstrated significantly enhanced SCG in H_2O using non-harmonic two-color laser fields. Compared to single-color or harmonic two-color configurations, these non-harmonic fields enable much broader spectral generation with substantially higher efficiency. This enhancement arises from the combined effects of soliton compression accompanied by RDW emission, phase- and group-velocity-matched cascaded FWM, and subsequent XPM. This work not only establishes a robust approach to achieving broader and more intense SCG, but also provide new potential for broadband/multicolor spectroscopy in liquids—particularly in H_2O —a rapidly emerging frontier in attosecond science and surface/interface physics.

Funding. This study was supported by JSPS KAKENHI Grant-in-Aid for Scientific Research (A) [22H00296], Grant-in-Aid for Scientific Research (B) [23H01877 and 23K26570], Grant-in-Aid for Challenging Research (Exploratory) [21K18896], ATLA Japan Innovative Science and Technology Initiative for Security [JPJ004596], JST-CREST [JPMJCR22L2], MATSUO FOUNDATION, Amada Foundation General research and development grant [AF-2021212-B2, AF-2022234-B3], the International Research Exchange Support Program of the National Institutes of Natural Sciences (NINS), Joint Research by NINS [01112104], and by the Special Project by Institute for Molecular Science [IMS programme 22IMS1101].

Disclosures. The authors declare no conflicts of interest.

REFERENCES

- R. R. Alfano and S. L. Shapiro, Phys. Rev. Lett. **24**, 584 (1970).
- E. L. Dawes and J. H. Marburger, Phys. Rev. **179**, 862 (1969).
- A. Dubietis and A. Couairon, *Ultrafast Supercontinuum Generation in Transparent Solid-State Media*, SpringerBriefs in Physics (Springer International Publishing, 2019).
- S. L. Chin, *Femtosecond Laser Filamentation*, vol. 55 of *Springer Series on Atomic, Optical, and Plasma Physics* (Springer New York, New York, NY, 2010).
- W. Liu and S. Chin, Opt. Express **13**, 5750 (2005).
- J. Marburger, Prog. Quantum Electron. **4**, 35 (1975).
- T. Kanai, Y. Lee, M. Seo, and D. E. Kim, J. Opt. Soc. Am. B **36**, 2407 (2019).
- T. Kanai, P. Malevich, S. Kangaparambil, K. Ishida, M. Mizui, K. Yamanouchi, H. Hoogland, R. Holzwarth, A. Pugžlys, and A. Baltuška, Opt. Lett. **42**, 683 (2017).
- M. T. Hassan, T. T. Luu, A. Moulet, O. Raskazovskaya, P. Zhokhov, M. Garg, N. Karpowicz, A. M. Zheltikov, V. Pervak, F. Krausz, and E. Goulielmakis, Nature **530**, 66 (2016).
- T. Udem, R. Holzwarth, and T. W. Hänsch, Nature **416**, 233 (2002).
- H. N. Paulsen, K. M. Hilligse, J. Thøgersen, S. R. Keiding, and J. J. Larsen, Opt. Lett. **28**, 1123 (2003).
- E. Goulielmakis, V. S. Yakovlev, A. L. Cavalieri, M. Uiberacker, V. Pervak, A. Apolonski, R. Kienberger, U. Kleineberg, and F. Krausz, Science **317**, 769 (2007).
- A. Zheltikov, J. Opt. Soc. Am. B **36**, A168 (2019).
- T. Popmintchev, M.-C. Chen, D. Popmintchev, P. Arpin, S. Brown, S. Ališauskas, G. Andriukaitis, T. Balčiūnas, O. D. Mücke, A. Pugžlys, A. Baltuška, B. Shim, S. E. Schrauth, A. Gaeta, C. Hernández-García, L. Plaja, A. Becker, A. Jaron-Becker, M. M. Murnane, and H. C. Kapteyn, Science **336**, 1287 (2012).
- E. J. Takahashi, P. Lan, O. D. Mücke, Y. Nabekawa, and K. Midorikawa, Phys. Rev. Lett. **104**, 233901 (2010).
- Y. Nomura, T. Kanai, S. Minemoto, and H. Sakai, Phys. Rev. A **75**, 041801(R) (2007).
- P. Béjot, G. Karras, F. Billard, E. Hertz, B. Lavorel, E. Cormier, and O. Faucher, Phys. Rev. Lett. **112**, 203902 (2014).
- N. Garejev, V. Jukna, G. Tamošauskas, M. Veličkė, R. Šuminas, A. Couairon, and A. Dubietis, Opt. Express **24**, 17060 (2016).
- C. R. Loures, A. Armaroli, and F. Biancalana, Opt. Lett. **40**, 613 (2015).
- M. Vengris, N. Garejev, G. Tamošauskas, A. Čepėnas, L. Rimkus, A. Varanavičius, V. Jukna, and A. Dubietis, Sci. Rep. **9**, 9011 (2019).
- A. V. Mitrofanov, A. A. Voronin, S. I. Mitryukovskiy, D. A. Sidorov-Biryukov, A. Pugžlys, G. Andriukaitis, T. Flöry, E. A. Stepanov, A. B. Fedotov, A. Baltuška, and A. M. Zheltikov, Opt. Lett. **40**, 2068 (2015).
- N. Aközbek, A. Iwasaki, A. Becker, M. Scalora, S. L. Chin, and C. M. Bowden, Phys. Rev. Lett. **89**, 143901 (2002).
- Y. Nomura, Y.-T. Wang, A. Yabushita, C.-W. Luo, and T. Fuji, Opt. Lett. **40**, 423 (2015).
- D. J. Cook and R. M. Hochstrasser, Opt. Lett. **25**, 1210 (2000).
- Y. Zheng, Z. Zeng, X. Li, X. Chen, P. Liu, H. Xiong, H. Lu, S. Zhao, P. Wei, L. Zhang, Z. Wang, J. Liu, Y. Cheng, R. Li, and Z. Xu, Opt. Lett. **33**, 234 (2008).
- J. Zhao, L. Guo, W. Chu, B. Zeng, H. Gao, Y. Cheng, and W. Liu, Opt. Lett. **40**, 3838 (2015).
- T. Kanai and H. Sakai, J. Chem. Phys. **115**, 5492 (2001).
- F. Théberge, N. Aközbek, W. Liu, A. Becker, and S. L. Chin, Phys. Rev. Lett. **97**, 023904 (2006).
- S. Junaid, J. Hofmann, M. Chemnitz, M. Blothe, F. Setzpfandt, S. Nolte, and M. A. Schmidt, APL Photonics **9**, 016114 (2024).
- W. Liu, L. Zhu, L. Wang, and C. Fang, Opt. Lett. **38**, 1772 (2013).
- T. R. Ensley, D. A. Fishman, S. Webster, L. A. Padilha, D. J. Hagan, and E. W. Van Stryland, Opt. Express **19**, 757 (2011).
- K. Wang, L. Qian, H. Luo, P. Yuan, and H. Zhu, Opt. Express **14**, 6366 (2006).
- F. Leo, S.-P. Gorza, J. Safioui, P. Kockaert, S. Coen, U. Dave, B. Kuyken, and G. Roelkens, Opt. Lett. **39**, 3623 (2014).
- G. Genty, M. Lehtonen, and H. Ludvigsen, Opt. Express **12**, 4614 (2004).
- P. Vasa, J. A. Dharmadhikari, A. K. Dharmadhikari, R. Sharma, M. Singh, and D. Mathur, Phys. Rev. A **89**, 043834 (2014).
- R. Šuminas, G. Tamošauskas, G. Valiulis, and A. Dubietis, Opt. Lett. **41**, 2097 (2016).
- P. Panagiotopoulos, P. Whalen, M. Kolesik, and J. V. Moloney, Nat. Photonics **9**, 543 (2015).
- A. M. Heinzerling, F. Tani, M. Agarwal, V. S. Yakovlev, F. Krausz, and N. Karpowicz, Nat. Photonics **19**, 772 (2025).
- J. A. Dharmadhikari, G. Steinmeyer, G. Gopakumar, D. Mathur, and A. K. Dharmadhikari, Opt. Lett. **41**, 3475 (2016).
- I. Pupeza, M. Huber, M. Trubetskov, W. Schweinberger, S. A. Hussain, C. Hofer, K. Fritsch, M. Poetzlberger, L. Vamos, E. Fill, T. Amotchkina, K. V. Kepesidis, A. Apolonski, N. Karpowicz, V. Pervak, O. Pronin, F. Fleischmann, A. Azzeer, M. Žigman, and F. Krausz, Nature **577**, 52 (2020).
- T. Sugimoto, N. Aiga, Y. Otsuki, K. Watanabe, and Y. Matsumoto, Nat. Phys. **12**, 1063 (2016).
- T. Kanai, C. Jin, H. Tsunekawa, A. Sakurai, and T. Sugimoto, "Anomalous lifetime of optical phonons in graphene at buried interfaces," in *2025 Conference on Lasers and Electro-Optics Europe & European Quantum Electronics Conference (CLEO/Europe-EQEC)*, (IEEE, 2025),

pp. EI–2.4.

43. A. Tcypkin, M. Zhukova, M. Melnik, I. Vorontsova, M. Kulya, S. Putilin, S. Kozlov, S. Choudhary, and R. W. Boyd, *Phys. Rev. Appl.* **15**, 054009 (2021).
44. S. R. Pattenau, L. M. Streacker, and D. Ben-Amotz, *J. Raman Spectrosc.* **49**, 1860 (2018).
45. S. Kedenburg, M. Vieweg, T. Gissibl, and H. Giessen, *Opt. Mater. Express* **2**, 1588 (2012).
46. Y. Chen, *J. Opt. Soc. Am. B* **7**, 43 (1990).
47. R. W. Boyd, *Nonlinear optics*, 4th ed. (Elsevier, San Diego, 2020), p. 208.